Energy management of implantable cardioverter-defibrillators using auxiliary power transfer

Abdollah Hosseinnia[a], Bahador Makkiabadi*[b], Hossein Ahmadi-Danesh-Ashtiani[c], Ahmad Khoshgard[d]

a Department of Energy Systems Engineering, Faculty of Engineering, South Tehran Branch, Islamic Azad University, Tehran, Iran

b Department of Medical Physics and Biomedical Engineering, School of Medicine, Tehran University of Medical Sciences, Tehran, Iran

c Department of Energy and Mechanical Engineering, Faculty of Engineering, South Tehran Branch, Islamic Azad University, Tehran, Iran

d Research Center for Biomedical Technologies and Robotics (RCBTR), Advanced Medical Technologies and Equipments Institute (AMTEI), Tehran, Iran

* Corresponding author: Bahador Makkiabadi, Email: b-makkiabadi@tums.ac.ir

Accepted by Scientia Iranica

Abstract

Implantable cardioverter-defibrillators (ICDs) are among the most frequently used internal battery-powered implantable systems, allowing for the permanent monitoring of heart signals and inducing cardiac shocks in the event of heart arrhythmias. Evidently, a considerable portion of the system's energy is lost when an electric shock occurs, or the system is prepared to induce an electric shock (by charging the battery), shortening the ICD service life. Then, the system should be surgically replaced in a short time. Contrary to the previous works, this study introduces a novel technique to manage and compensate for the internal energy of ICDs and develop complementary energy channels through optimized inductive links. Different inductive drivers are analyzed and compared based on the physical ICD conditions to design an efficient auxiliary inductive wireless energy transfer system. A comparison of wireless power transfer scenarios indicated that power transfer using electromagnetic field induction and coupling coils was optimal. This study also aims to simultaneously enhance the coupling factor and quality factor of the coils by employing geometric optimization in coil width, spacing, and number of turns. The analytical and simulation models were validated, and the experimental results demonstrated a maximum WPT efficiency of 51%, which outperforms similar works reported in recent literature.

Keywords: Electric shock, Defibrillation, Wireless power transfer, Coils.

1. Introduction

Globally, sudden cardiac death (SCD) is a leading cause of death, particularly in Western countries. The major cause of SCD is excessively high or low heart rates [1]. It is common for an ICD shock to be unanticipated when ventricular tachycardia (VT) results in a shock from an implantable cardioverter-defibrillator (ICD) [2]. There are 350,000 sudden cardiac deaths out-of-hospital each year in the U.S. [3]. In the last few decades, due to the growth of the microelectronics industry and semiconductor technology, electronic devices have not only become smaller but also

more complex and have played a vital role in human life [4]. The main advantage of these systems is the elimination of batteries or their minimization, reducing the cost and making them more suitable for the environment [5]. Advancements in the miniaturization of high-density power sources, electronic circuits, and communication technologies enabled the construction of miniaturized electronic devices implanted directly in the heart [6]. It has become increasingly important to prevent sudden cardiac death by utilizing implantable cardioverter-defibrillators (ICDs). [7]. By transmitting voltage shocks, an ICD can detect hazardous fibrillation-induced high heart rates and restore a natural heart rate, reducing SDC mortality rates in light of the permanent protection it offers [8]. However, Successful defibrillation by an ICD depends on its ability to deliver shocks that exceed the defibrillation threshold [9]. According to the literature, two-chamber ICDs have an average longevity of nearly six years, while three-chamber ones are five years. Longevity is often a significant factor associated with battery discharge replacement.

Patient longevity is disproportionate to that of the implantable cardiac devices [10]. Recent advances (2023–2025) in wireless power transfer for implantable devices have focused on improving transfer efficiency, patient safety, and miniaturization. Leading studies have demonstrated the use of resonant inductive links and adaptive frequency tuning to overcome positional misalignment and tissue attenuation. Wireless power transmission experiments in implantable monitoring systems have demonstrated that flat spiral receiver coils, when optimized for geometry and resonance, can achieve transfer efficiencies up to 60% in simulation and approximately 60% experimentally through biological tissue at around the resonant frequency, even with increased tissue thickness compared to the model [11], while Buchmeier et al. proposed an optimized near-field communication (NFC) wireless power transfer system at 13.56 MHz using rectangular printed spiral coils, demonstrating stable performance across a defined free-positioning charging area through combined geometric design and circuit-level [12]

Wireless power transfer (WPT) offers an ideal solution that eliminates the need for invasive surgery and ensures patient safety at the same time [13]. Different energy resources were evaluated. Research has shown that the limited power per unit area is the major disadvantage of energy supply techniques. Therefore, larger systems are required to receive higher output power. Using coupled magnetic coils to transfer energy proved to be the most efficient method [14]. Self-inductance, mutual inductance, and coupling coefficient were calculated for this purpose [15]. Different drivers were analyzed and compared to maximize the coupling and quality factors of the coils to obtain an efficient remote power link. The coils were geometrically optimized in size, spacing, and number of turns.

In addition, Detka et al. extensively investigated wireless power transfer schemes for various implantable medical devices, including cardiac pacemakers and neurostimulators. Their research emphasized the influence of coil geometry, alignment, and tissue properties on achievable transfer efficiency. They reported transfer rates of up to 23% using state-of-the-art planar coils for subcutaneous implants. The present study builds upon these findings, validating the impact of

Accepted by Scientia Iranica

geometric optimization, but notably surpasses Detka's reported efficiency by approximately 28%, thus establishing a new performance benchmark for ICD applications [16].

2. Materials and methods

In this section, we discuss auxiliary power transfer as an effective means of managing energy within ICDs. ICDs should be replaced when the battery is expired. Low-power electronic devices are required to lengthen the longevity of an ICD and reduce the number of invasive surgeries. In addition, patients can benefit from WPT instead of skin-through wires to help them move more easily and to protect their health. WPT circuits have three components in their main block diagram: the power amplifier, inductive link, and a rectifier on the receiver side to convert AC voltage into DC voltage, as shown in Fig. 1.

The amplifier power circuit is powered by the battery and used as the sinusoidal current or sinusoidal source. The sinusoidal signals of the power amplifier are transmitted to the second component of WPT (*i.e.*, inductive link). The inductive link induces current from the transmitter to the receiver. The sinusoidal signals are received from the first component, generating an electromagnetic field. A sinusoidal current is induced within the receiver once the second component (receiver) is near the electromagnetic field. Then, a voltage rectifier on the receiver side converts the AC signal into DC. As a result, the DC voltage is received from the battery and delivered to the consumer. The two coils are positioned at a certain distance from each other, as shown in Figure 2. The second coil is typically smaller due to spatial limitations, and coil spacing depends on the skin thickness.

WPT system design begins with the innermost component and ends with the outermost one.

2.1. Rectifier

the rectifier, a key component that converts AC to DC[17]. It is required to find its total equivalent resistant $R_{load.ac}$, *as* shown in Fig. 3, to calculate the power loss during optimization in the rectifier, which is a nonlinear circuit. Let V_{L2} be the potential difference across the inductor. Then, based on the power principle, the output power is given by:

$$P_{dc} \approx \frac{\left(V_{load,dc}\right)^2}{R_{load,dc}} + \left| \frac{\left(V_{diode}.V_{load,dc}\right)}{R_{load,dc}} \right| \quad (1)$$

$$P_{ac} = \frac{\left(V_{L2}\right)^2}{2R_{load,ac}} = \left| \frac{\left(V_{load,dc} + V_{diode}\right)^2}{2R_{load,ac}} \right|$$

$$V_{L2} = V_{diode} + V_{Load,dc} \quad (2)$$

As the diode voltage V_{diode} (forward voltage of the diode) and $V_{load,dc}$ are known, V_{L2} is obtained and inserted in *Eq.* (3) to obtain $R_{load,ac}$ as:

Accepted by Scientia Iranica

$$R_{load.ac} = \frac{\left(V_{diode}.V_{load.dc}\right)^2}{2\left(\frac{\left(V_{DC}\right)^2}{R_{dc}} + \frac{V_{diode}.V_{load.dc}}{R_{dc}}\right)} \quad (3)$$

R_{dc} is *280* Ω for V_D=1 V and $V_{1,2}$=*7 V*. Then, the equivalent voltage of $R_{load.ac}$ can be used for simplification.

2.2 Optimal power transfer frequency

The frequency, a crucial factor in implementing efficient WPT, is to maximize the induced voltage on the implant side. As the primary side frequency ω_1 and secondary side frequency ω_2 operate together, their peaks should be in the same region. In fact, with known L_2, L_2, and R_L, C_1 and C_2 should be at the same frequency to achieve maximum efficiency. Based on Kirchhoff's Voltage Law (KVL), the oscillation frequency (ω) or its resonance is obtained as:

$$\omega_1 = \omega_2 = \omega_c = \frac{1}{\sqrt{L_1C_1}} = \frac{1}{\sqrt{L_2C_2}} \quad (4)$$

2.2. Inductive link

Figure 4 schematically depicts the induction path, where R_{p1} is the resistance of inductor L_1 (or parasite resistance). V_{req} is the equivalent voltage in the inductive link of the primary side. The equivalent resistivity on the primary side should be calculated to analyze the induction path. In this figure, R_{refl2} is equivalent to resistance in the inductive link of the secondary side, and V_{refl2} is equivalent to voltage in the inductive link of the secondary side.

Based on KVL and Kirchhoff's Circuit Law (KCL), the observed impedance is given by, $Z_T = R_{refl2}$ Equivalent resistance of inductive link and rectifier:

$$Z_T = R_{refl2} = \frac{\left(M_{12}\omega_c\right)^2}{\frac{\left(L_2\omega_c\right)^2}{R_L} + R_{p_2}} \quad (5)$$

$$K_{12} = \frac{M_{12}}{\sqrt{L1L2}} \quad (6)$$

where M is dependent on K_{12}, L_1, and L_2, and K reflects the effect of the coupling inductor on the transmitter and receiver sides, which is dependent on coil spacing and shape. Here, M is found through K, L_1, and L_2, obtaining Z_T. Hence, Z_T can represent the inductive link. A voltage source is on the primary side, and a voltage is applied to the secondary side. Since there is a load on the receiver side, Z_T is applied to the transmitter side. The efficiency of the inductive link is obtained as the ratio of the output power to input power [18]:

Accepted by Scientia Iranica

$$ {}_1\eta_2 = \frac{Q_1 Q_2 K_{12}^{\ 2}}{1+Q_1 Q_2 K_{12}^{\ 2}} \frac{Q_2}{Q_2+Q_{RL}} \quad (7) $$

$\eta_{link} = \eta$

$$ Q_{RL} = R_L C_2 \omega_c = \frac{R_L}{L_{21}\omega_c} \ , \ \omega_1 = \omega_2 = \omega_C \quad (8) $$

As can be seen, Q is higher when R_L is lower. Thus, the efficiency is dependent on Q as Q affects R. The efficiency also depends on K, which is dependent on the primary to secondary positions, determining a portion of the magnetic field on the receiver side. The wire shows impedance and resistance once it receives a sinusoidal current. The resistance changes as the number of turns increases, changing L and Q. An increased number of turns would also change K. The factors with the largest effect on K are coil spacing and inductor diameter (d_{out}) [19]:

$$ M \cong \frac{\mu_0 N_T \left(d^2_{out.T}\right) N_R \left(d^2_{out.R}\right) \pi}{2\sqrt{\left(d^2_{out.R}+X^2\right)^3}} \quad (9) $$

This indicates that smaller coil spacing leads to a stronger electromagnetic field and a larger K. Furthermore, a larger inductor diameter enables higher power transfer. Thus, the maximum inductor diameter is applied, depending on user-defined constraints.

Different coupled coils with optimized geometrical parameters were designed to find the optimal location for WPT. Some such parameters were constrained by coil spacing S, and outer inductor diameter d_{out}. The input resistance of the rectifier circuit is designed by simulation. The remaining parameters should be set carefully for optimal remote power linking. Table 1 reports the WPT design parameters.

describes the table of fixed design parameters determining the maximum magnetic resistance by the optimal outer diameter of the power transmission coil (*dout*).

The optimal d_{out} is calculated to be 40 mm. Thus, coil spacing equals S=5 mm, with the K-coefficient being found as 0.3 using N and d. The circuit can be designed based on these parameters. The objective is efficiency maximization. Efficiency is dependent on K, L_1, L_2, Q_1, and Q_2 [20]:

$$ {}_1\eta_2 = \frac{Q_1 Q_2 K_{12}^{\ 2}}{1+Q_1 Q_2 K_{12}^{\ 2}} \frac{Q_2}{Q_2+Q_{RL}} \quad (10) $$

$\eta_{link} = \eta$

It is required to find S, W, and N to calculate d_{in}. Once d_{out} and S have been obtained, W, N, and d_{in} are to be found. W is assumed to be 0.5. Then, d_{in} is found for a given N as:

$$ d_{in} = d_{out} - 2N(W+S) \quad (11) $$

Accepted by Scientia Iranica

Finally, d_{in} and d_{out} were obtained to be 10 and 40 mm for the external component, while 7 and 25 mm for the internal component, respectively. Once N, S, W, W, N_2. d_{in}, and d_{out} have been found, L_2, R_{dc}, R_{ac}, and Q_2 are obtained. A total of N scenarios are assumed for the secondary side, identifying the optimal scenario. Finally, the coil is designed with a certain R_1, R_2, L_1, and L_2. However, a coil configuration is required to cover the entire coil. Figure 6 shows the optimized coupled coils and coil configuration.

2.4 Class-E power amplifier

Power inverters are essential converter systems that are characterized by changing DC powers to AC powers [21]. Class-E power amplifiers have good, reliable efficiency in implementation (up to 100% theoretical efficiency) [24]. In addition, they are known as link stimulators for implantable systems [22, 23]. Class-E amplifiers have a simpler structure than other power amplifiers [24]. A class-E amplifier is a simple oscillating circuit with low complexity and reduces power consumption compared to other amplifiers. Therefore, the present work adopted a class-E amplifier for WPT. Figure 7 depicts a schematic of a class-E power amplifier with a wireless power link.

The maximum output power transferred to the load is calculated as follows [25]:

$$P_{out} = \frac{2}{1+\left(\frac{\pi^2}{4}\right)} \cdot \frac{V^2_{sup}}{R_L} \tag{12}$$

However, there are losses in the amplifier circuit due to non-ideal organic elements, *e.g.*, link transistor on-resistance R_{ON} and suppressor inductor parasite resistance. The measured power efficiency of the amplifier is nearly 80-85% due to the losses in the transmitter and receiver. Let us evaluate the WPT system using Z_T or $R_{reflected}$ and V_{relf2} in simulation settings. Figure 8 shows the WPT system, where V_{out} and V_{ref12} can be calculated as:

$$\left|V_{out}\right| = \frac{1}{K_{12}}\sqrt{\frac{L_2}{L_1}}\frac{Q_{RL}}{\sqrt{1+Q^2_{RL}}}\left|V_{ref\,12}\right| \tag{13}$$

According to Fig. 9 and Eqs. (14) and (15), full resonance would not occur. As a result, imaginary impedance j_x remains.

$$i_o = \frac{C}{R}\sin(\theta+\varphi);\ \theta = \omega t \tag{14}$$

$$V_O = C\sin(\theta+\varphi);\ \ \theta = \omega t \tag{15}$$

The imaginary impedance j_x is determined by the capacitance C_0 or C_1 – since L_0 has been found, while C_0 and C_1 are unknown. Figure 10 illustrates a completely nonlinear circuit. This circuit is solved under some assumptions, including:

Accepted by Scientia Iranica

1) The *100μH* inductor has no *DC* drop,
2) Current i_{DC} flows through the inductor as it is large,
3) Once $i_{sin\theta}$ flows through it, the capacitor is charged by i_{dc}-i_0. Then, the charging of the capacitor can be written as:

$$v_{(\theta)} = \frac{1}{B}\int_{0}^{\theta}\left[1-\frac{C}{R}\sin(u+\varphi)\right]du = \frac{1}{B}\theta+\frac{C}{BR}\left(\cos(\theta+\varphi)-\cos(\varphi)\right);B=\omega C \quad (16)$$

$$P_O = Pi \rightarrow \frac{C^2}{2R} = \frac{V_{cc}^2}{R_{dc}} \quad (17)$$

$$v(\pi) = 0 \quad (18)$$

$$\left.\frac{dv(\theta)}{d(\theta)}\right|_{\theta=\pi} = 0 \quad (19)$$

Eq. (17) is the fundamental equation of class-E power amplifiers, which gives *θ, C*, and V_0. Here, $V_{(\theta)}$ is known. Furthermore, $V_{(\theta)}$ is sinusoidal, representing the voltage across capacitor *C*. The capacitor is charged at i_{dc}-i_0, and the capacitor charge equation was written. The first component of this remote signal is obtained in two ways:

First equation:$(j_x+R)i_0=V_0$

Second equation: the Fourier series of $V_{(\theta)}$ is written, and the first component becomes sinusoidal

Third equation: As it is sinusoidal, no cosine component exists. Then, the cosine component of the Fourier series is set equal to zero.

Fourth equation: Once V_{CC} and an inductor exist, no R_{dc} exists for an ideal inductor, and V_{CC} drops to the bottom point. Then, the average $V_{(\theta)}$ is V_{CC}. The system of four equations with four unknowns is solvable. In the design, R and V_R are known based on user-defined data. Here, C_0 and C_2 are to be set to maximize efficiency. At a frequency of 10 MH, the switch has losses. For a scenario where the voltage and current overlap in time when either the voltage is zero, and current is non-zero or the current is zero, and voltage is non-zero; that is, the product of voltage and current is zero, and no power is consumed. Then,

$$i \times V_{cc} = \frac{V_O}{2R} \quad (20)$$

As a result, battery power is given by:

$$Battery\ Power = i \times V_{cc} \quad (21)$$

Then, apart from those four equations, three more equations are included.

First equation:

Accepted by Scientia Iranica

$$v(\pi) = 0 \tag{22}$$

The voltage becomes zero in the middle of the cycle as there is a current. Then, if the frequency is on for T1 seconds, it is off for T1 seconds, as shown in Fig. 11.

There is a current when the switch is on, and there is no current when the switch is off. Furthermore, there is a voltage when the switch is off, and there is no voltage when the switch is on. Then,

$$v(\pi) = 0 \tag{23}$$

The second equation:

According to Figure 12, voltage slope versus time is important because voltage increases as slope increases.

It is required that $\left.\frac{dv(\theta)}{d(\theta)}\right|_{\theta=\pi} = 0$ to neutralize the timing effect. The voltage is high when the slope is high, while it is low when the slope is low.

Third equation:

$$P_O = Pi \rightarrow \frac{C^2}{2R} = \frac{V^2_{cc}}{R_{dc}} \tag{24}$$

The efficiency maximization conditions of these three equations are added to the four previous equations. Then, C_1 and C_0 are related to R as:

$$C_0 = \frac{1}{5.4466\omega_c R_{eq}} \tag{25}$$

$$C_1 = \frac{1}{\omega^2_C\left(L_1 - \frac{X_1}{\omega_c}\right)}; X_1 = 1.1552R_{eq} \tag{26}$$

Then, X_1 is obtained and inserted into *Eq*. (26) to find C_1. As a result, V_{CC} and $V_{Rectifier}$ are directly related.

L is set to a high value (e.g., 100 m) as I_{dc} is almost constant. As a result, a power of 100-150 mW is applied (higher power is impossible due to limitations). In Fig. 13, R_{ds} denotes transistor resistance.

Here, R_{ds} is added to the inductor resistance. For example, when R_L=5 Ω and R_{dc}=4 Ω, the total resistance is 9 Ω.

3. Results and Discussion

Accepted by Scientia Iranica

Table ۲ summarizes the main WPT design parameters utilized in this study.

As observed in Table X, the present study demonstrates superior experimental efficiency (51%) compared to prior works (typically below 35%) on similar ICD or implantable WPT systems, due to advanced coil optimization and improved link circuitry.

The data were introduced to MATLAB software, finding the inductor link to have an efficiency of 80% with R_{dc} and no rectifier.

In Fig. 14, V_{CC} = 4 and I = 43 mA, leading to a V_{max} of 15.129 V. Here, V_{max} is the voltage across the collector. Figure 15 indicates the simulation circuit in LTSpice for V_{CC}=3.3 V.

Figure 16 shows the steady-state output voltage simulated in LTSpice after discarding initial transients. The voltage form was sinusoidal, with an amplitude of 13 V, a current of 120 mA, and an efficiency of 81% in the absence of the rectifier and 77% in the presence of the rectifier.

Figure 17 depicts the transistor voltage (blue) and base voltage (green).

Figure 18 shows the transistor current (blue) and base current (green). Furthermore, the blue current is almost zero when the transistor is off.

Figure 19 represents the experimental results, where the first ammeter 3 mA, corresponds to the buffer, 41 mA corresponds to the E-class power amplifier's V_{CC} = 3.3 V. Here, the oscilloscope power voltage was 3.3 V. The power voltage of the E-class power amplifier was 3.3 V, with an experimental efficiency of 76.25. The efficiency was obtained to be 70.9% in the presence of the buffer.

Figure 20 plots the sinusoidal output, whereas Figure 21 depicts the base current and voltage. Here, 131.2 *mW* of power was received from the WPT circuit ($P_{in_{max}} = 3.2 \times 41 = 131.2\ mW$), and 100.04 *mW* of power was transferred to the load. Efficiency is defined as the ratio of output power to input power, which is calculated to be 76%.

Then, $P_{in_{max}} = 3.2 \times 53 = 169.6$ mW, and 92 mW of power was transferred to the load in the presence of the rectifier, leading to an efficiency of 54%. The efficiency was found to be 51% in the presence of the buffer. The experimental results confirm that the proposed WPT system provides a substantial leap in efficiency compared to prior solutions. Whereas most existing studies report efficiencies in the range of 10–34%, our configuration achieves 51%, which can extend device lifetime by at least 25–40% assuming typical duty cycles. This improvement is primarily attributed to geometric optimization of both the transmitter and receiver coils, as well as refining load matching techniques and adopting a class-E power amplifier. While the system performs effectively under ideal alignment, sensitivity to coil misalignment and tissue-induced loss remains a potential challenge, suggesting further exploration of adaptive tuning and closed-loop feedback in future designs.

3.1 Similar amplifiers

Accepted by Scientia Iranica

Researchers evaluated the Powering smart wireless implantable medical devices: Toward an internet of self-powered intra-body things.Traditional medical implants will be replaced by a new generation of implantable smart, reconfigurable devices endowed with sensing, processing, communication, and actuation capabilities.Earlier works studied the WPT of a deep brain stimulator[26].Earlier works studied the WPT of a deep brain stimulator. Their goal was to optimize the inductive link for recharging the deep brain stimulator's implantable pulse generator. The experimental data reported a WPT efficiency of 10.62% [27]. Researchers evaluated the feasibility of using an inductive link for WPT to a rechargeable implant in the chest. A WPT link was assumed between two flat coils, and its performance was evaluated through simulation and experimental tests. The maximum measured WPT efficiency was found to be nearly 23% [28]. An improved variant of the solution proposed in the present study was used in earlier works for WTP links of rechargeable pacemakers. The proposed link utilized a receiver integrated within the silicon header of a pacemaker. Based on the definition of the RF-to-RF efficiency, the link was found to have an efficiency of approximately 23%, based on the measured data. The link proposed in the present work had an efficiency of nearly 51% [29].

4. Conclusions

The present study aimed to prolong the longevity of ICDs using auxiliary power transfer. A WPT link was assumed between the two coils, and its performance was evaluated using simulation and experimental tests. The inductive link was employed to transfer the auxiliary power to the implanted ICD. The optimal transfer frequency was set to 10 MHz, and a class-E power amplifier was designed to achieve the optimum efficiency of the transmitter. Also, the performance and efficiencies of different parts of the power link are calculated and reported in detail. this study demonstrates that by leveraging advanced coil design and class-E amplifier technologies, the wireless power transfer efficiency for ICD applications can be improved from the 23–34% range typical in literature to over 50%. Such gains could result in up to 40% longer device lifespans before replacement surgery is needed, dramatically improving patient quality of life and reducing healthcare costs. We recommend that future work investigate integration with buck-boost DC-DC converters and explore real-time adaptive power tracking in clinical prototypes.

Acknowledgment

This research was supported by the Islamic Azad University, South Tehran Branch. It is the PhD thesis of the first author in Energy Systems Engineering at the Islamic Azad University of South Tehran Branch. The authors appreciate the supporters of the project.

References

Accepted by Scientia Iranica

1. Merchant, F.M., Quest, T., Leon, A.R. and El-Chami, M.F. "Implantable cardioverter-defibrillators at end of battery life: opportunities for risk (re)-stratification in ICD recipients", J. Am. Coll. Cardiol., 67(4), pp. 435-444 (2016). doi:10.1016/j.jacc.2015.11.033.

2. Ward, R.C., Desai, V.K., Cha, Y.M., Friedman, P.A. and Asirvatham, S.J. "Triggers and substrate: The whole is more than the sum of its parts—A case of implantable cardioverter-defibrillator shock induced with echocardiography", HeartRhythm Case Rep., 10(10), pp. 757-760 (2024). doi:10.1016/j.hrcr.2024.07.017.

3. Gessman, L.J., Schacknow, P.N. and Brindis, R.G. "Sudden Cardiac Death at Home: Potential Lives Saved With Fully Automated External Defibrillators",Ann. Emerg. Med., 83(1), pp. 35-41(2024). doi:10.1016/j.annemergmed.2023.08.006.

4. Arabyarmohammadi, N. and Ebrahimi, E. "A 20–200 mV, 92.52% peak efficiency, dual-mode boost converter with inductor peak-current-controlled and efficient ZCS for thermoelectric energy harvesting in bioimplantable devices", Microelectron. J., 135, pp. 105772 (2023). doi:10.1016/j.mejo.2023.105772.

5. Helalian, H., Pasandi, G. and Jafarabadi Ashtiani, S. "A robust low quiescent current power receiver for inductive power transmission in bio implants", Int. J. Electron., 104(5), pp. 761-774 (2017). doi:10.1080/00207217.2016.1244863.

6. Rav-Acha, M., Soifer, E. and Hasin, T. "Cardiac implantable electronic miniaturized and micro devices", Micromachines, 11(10), pp. 902 (2020). doi:10.3390/mi11100902.

7. van der Stuijt, W., Pepplinkhuizen, S., de Veld, J.A., Quast, A.B., van Halm, V.P., Bijsterveld, N.R., Nordkamp, L.O., Wilde, A.A., Smeding, L. and Knops, R.E. "Defibrillation threshold in elective subcutaneous implantable defibrillator generator replacements: Time to reduce the size of the pulse generator?", Int. J. Cardiol., 398, pp. 131639 (2024). doi: 10.1016/j.ijcard.2023.131639.

8. Kramer, D.B., Kennedy, K.F., Spertus, J.A., Normand, S.L., Noseworthy, P.A., Buxton, A.E., Josephson, M.E., Zimetbaum, P.J., Mitchell, S.L. and Reynolds, M.R. "Mortality risk following replacement implantable cardioverter-defibrillator implantation at end of battery life: Results from the NCDR®", Heart Rhythm, 11(2), pp. 216-221 (2014). doi: 10.1016/j.hrthm.2013.10.046.

9. Golzarian, H., Meyer, R.J., Carder, A.K. and Hakim, F.A. "Late malfunction of subcutaneous implantable cardioverter-defibrillator in a patient with advanced emphysema", HeartRhythm Case Rep., (online first) (2024). doi: 10.1016/j.hrcr.2024.04.006.

10. Zanon, F., Martignani, C., Ammendola, E., Menardi, E., Narducci, M.L., De Filippo, P., Santamaria, M., Campana, A., Stabile, G., Potenza, D.R. and Pastore, G. "Device longevity in a contemporary cohort of ICD/CRT-D patients undergoing device replacement", J. Cardiovasc. Electrophysiol., 27(7), pp. 840-845 (2016). doi:10.1111/jce.12990.

11. Schaufler, A., Sanin, A.Y., Sandalcıoglu, I.E., Hartmann, K., Croner, R.S., Perrakis, A., Wartmann, T., Boese, A., Kahlert, U.D. and Fischer, I."Concept of a fully-implantable system to monitor tumor recurrence", Sci. Rep., 13, 16362 (2023). doi:10.1038/s41598-023-43226-3.

12. Buchmeier, G.G., Takacs, A., Dragomirescu, D., Alarcon Ramos, J. and Fortes Montilla, A. "Optimized NFC circuit and coil design for wireless power transfer with 2D free-positioning and low load sensibility", Sensors, 21(23), 8074 (2021). doi:10.3390/s21238074.

Accepted by Scientia Iranica

13. Shaw, T., Mandal, B., Mitra, D., Rangaiah, P.K., Perez, M.D. and Augustine, R. "Metamaterial integrated highly efficient wireless power transfer system for implantable medical devices", AEU-Int. J. Electron. Commun., 173, pp. 155010 (2024). doi:10.1016/j.aeue.2023.155010

14. Ben Amar, A., Kouki, A.B. and Cao, H. "Power approaches for implantable medical devices", Sensors, 15(11), pp. 28889-288914 (2015). doi:10.3390/s151128889.

15. Ozupak, Y. and Cinar, M. "Analysis of a transformer designed for wireless power transmission system for different distance and alignment conditions and optimization with a developed algorithm", Scientia Iranica, (online first) (2024). doi:10.24200/sci.2024.63188.8268

16. Abduljaleel, H.K. and Gharghan, S.K. "Wireless power transfer-based single layer inductive coupling for biomedical implantable devices", In AIP Conf. Proc., Vol. 3232, No. 1, (AIP Publishing), pp. — (2024). doi: 10.1063/5.0236278.

17. Abiri, P., Abiri, A., Packard, R.R., Ding, Y., Yousefi, A., Ma, J., Bersohn, M., Nguyen, K.L., Markovic, D., Moloudi, S. and Hsiai, T.K. "Inductively powered wireless pacing via a miniature pacemaker and remote stimulation control system", Sci. Rep., 7(1), pp. 6180 (2017). doi:10.1038/s41598-017-06493-5.

18. Yang, F. and Wang, D. "IoT-enabled intelligent fault detection and rectifier optimization in wind power generators", Alexandria Eng. J., 116, pp. 129-140 (2025). doi: 10.1016/j.aej.2024.12.033.

19. Haerinia, M. and Shadid, R. "Wireless power transfer approaches for medical implants: A review", Signals, 1(2), pp. 209-229 (2020). doi: 10.3390/signals1020012.

20. Sokal, N.O. and Sokal, A.D. "Class EA new class of high-efficiency tuned single-ended switching power amplifiers", IEEE J. Solid-State Circuits, 10(3), pp. 168-176 (1975). doi: 10.1109/JSSC.1975.1050582.

21. Eya, C.U., Salau, A.O. and Omeje, C.O. "Performance analysis of mono-stage three-phase DC-AC converter with reduced logic power supply circuits", Scientific African, 26, pp. e02421 (2024). doi: 10.1016/j.sciaf.2024.e02421.

22. Troyk, P.R. and Schwan, M.A. "Closed-loop class E transcutaneous power and data link for microimplants", IEEE Trans. Biomed. Eng., 39(6), pp. 589-599 (1992). doi: 10.1109/10.141197.

23. Kendir, G.A., Liu, W., Wang, G., Sivaprakasam, M., Bashirullah, R., Humayun, M.S. and Weiland, J.D. "An optimal design methodology for inductive power link with class-E amplifier", IEEE Trans. Circuits Syst. I: Reg. Papers, 52(5), pp. 857-866 (2005). doi: 10.1109/TCSI.2005.846208.

24. Silay, K.M. "Remotely powered wireless cortical implants for brain-machine interfaces", Ph.D. Thesis, Ecole Polytechnique Fédérale de Lausanne (EPFL), Switzerland (2012).

25. Lee, T.H. The design of CMOS radio-frequency integrated circuits, 2nd Edn., Cambridge University Press, Cambridge, UK (200٤).

26. Guida, R. and Melodia, T. "Powering smart wireless implantable medical devices: Toward an internet of self-powered intra-body things", Ad Hoc Netw., pp. 103748 (2025). doi: 10.1016/j.adhoc.2024.103748.

27. Monti, G., De Paolis, M.V. and Tarricone, L. "Wireless energy link for deep brain stimulation", In Proc. Eur. Microwave Conf. (EuMC), pp. 64-67 (2015). doi: 10.1109/EuMC.2015.7345700.

28. Monti, G., De Paolis, M.V., Corchia, L. and Tarricone, L. "Wireless resonant energy link for pulse generators implanted in the chest", IET Microw. Antennas Propag., 11(15), pp. 2201-2210 (2017). doi: 10.1049/iet-map.2017.0250.

Accepted by Scientia Iranica

29. Monti, G., De Paolis, M.V., Corchia, L., Tarricone, L. and Mongiardo, M. "Wireless power link for rechargeable pacemakers", In Proc. IEEE MTT-S Int. Microwave Workshop Series Adv. Mater. Process. RF THz Appl. (IMWS-AMP), pp. 1-3 (2017). doi:10.1109/IMWS-AMP.2017.8247433.

List of Figure Captions

List of Table Captions

Accepted by Scientia Iranica

Table 1. WPT parameters.

Table ۲. Quantitative comparison of state-of-the-art inductive power transfer solutions for ICD and related implants.

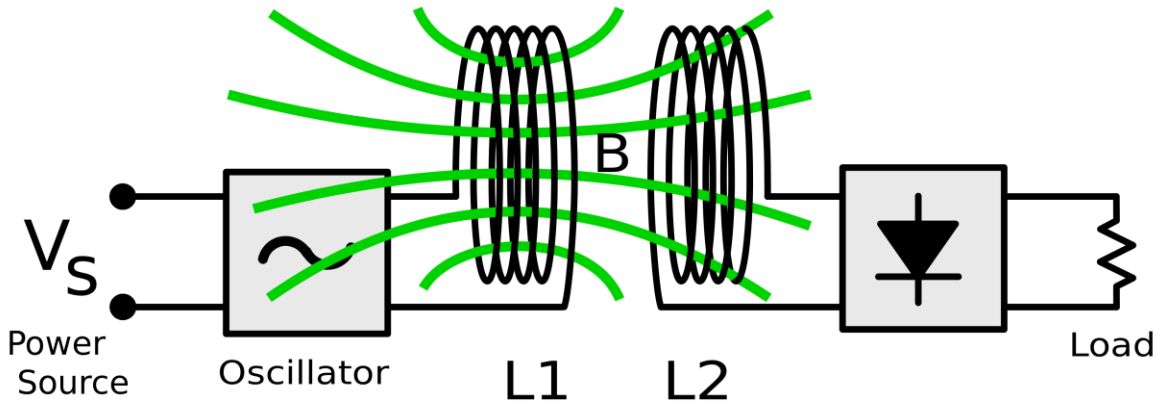

Fig. 1. WPT block diagram[25].

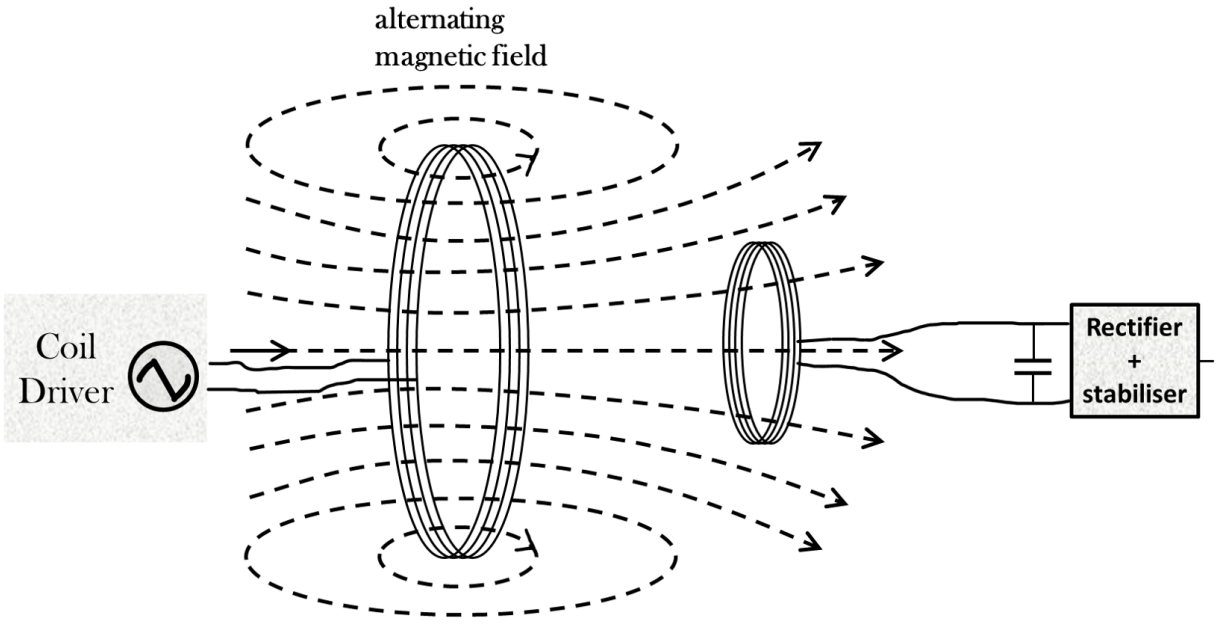

Fig. 2. Schematic of induction and rectification[25].

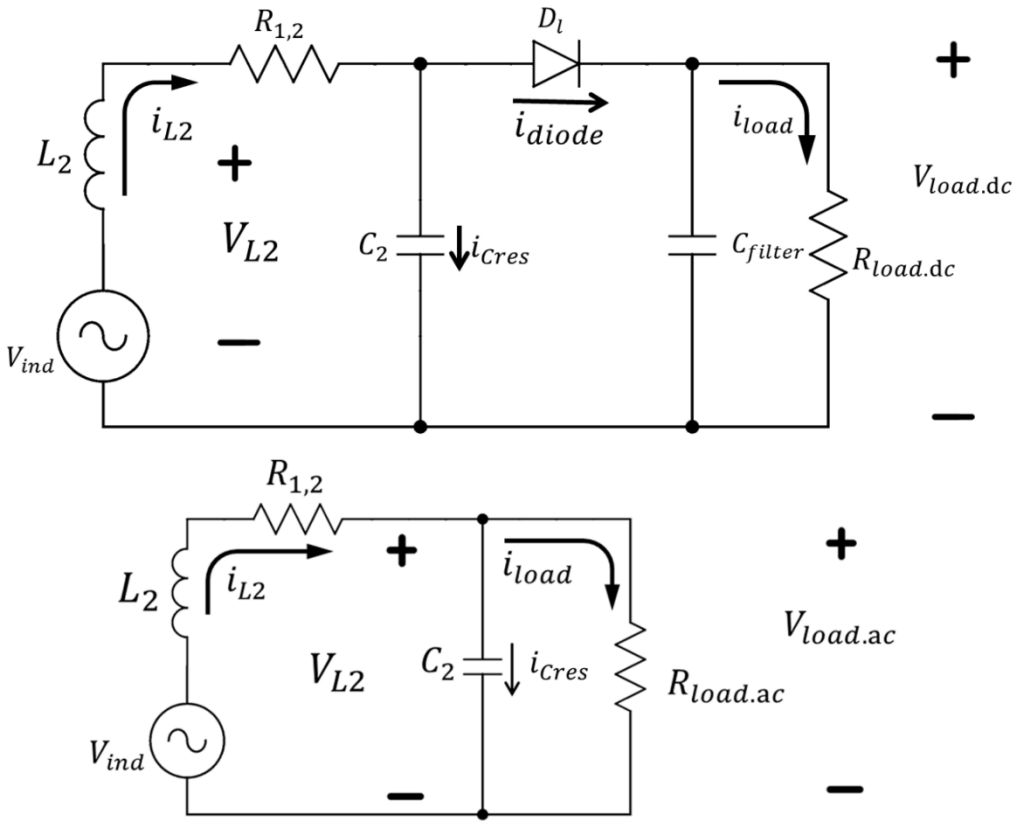

Fig. 3. Rectifiers to generate a DC output from an AC input

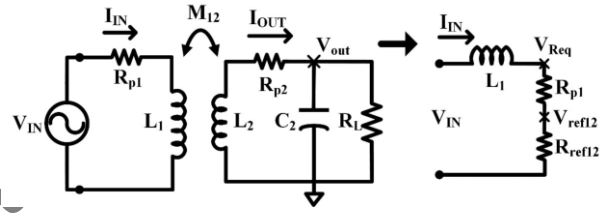

Fig. 4. Induction block diagram

Accept

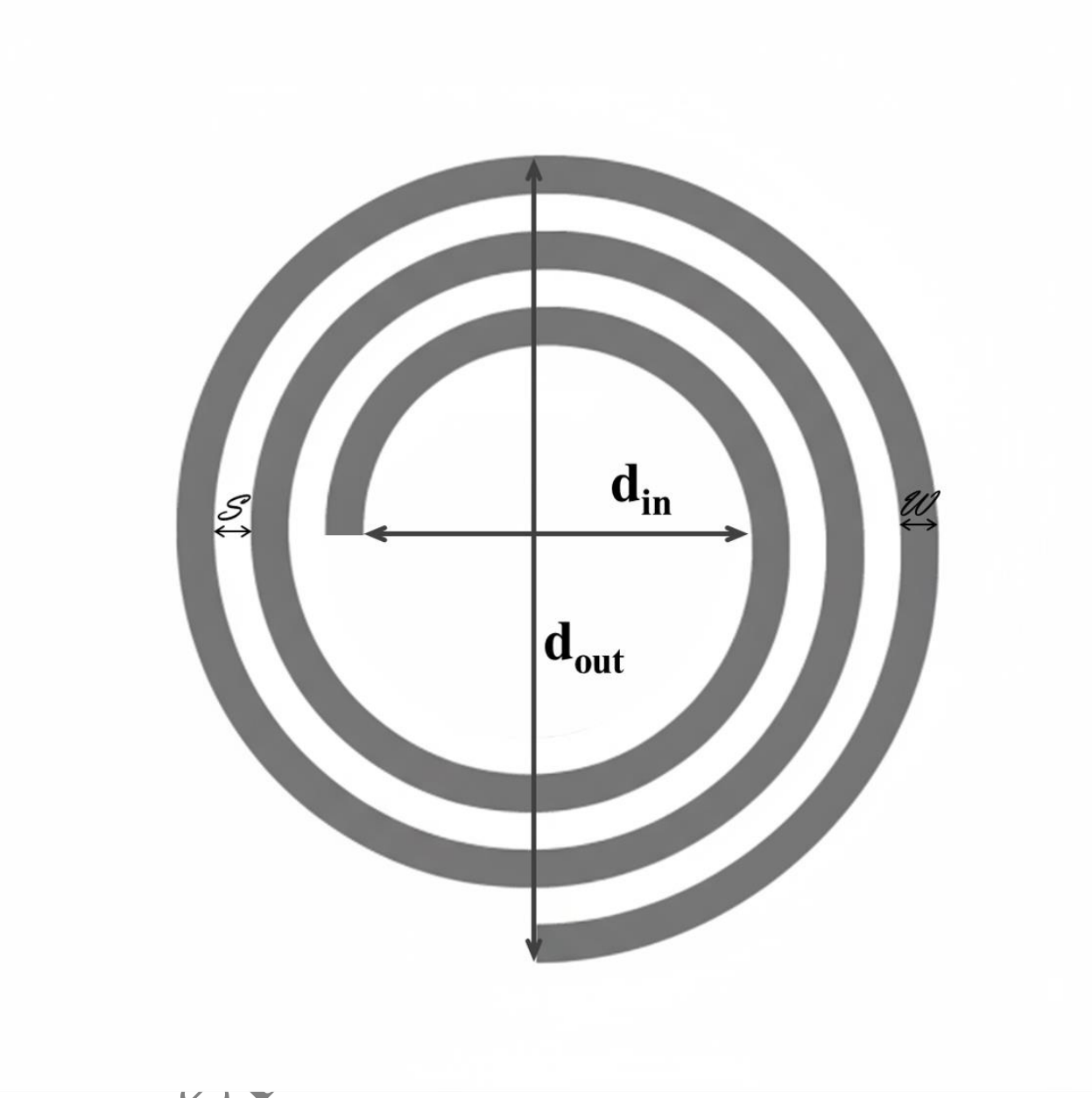

Fig. 5. Schematic view of coil shape.

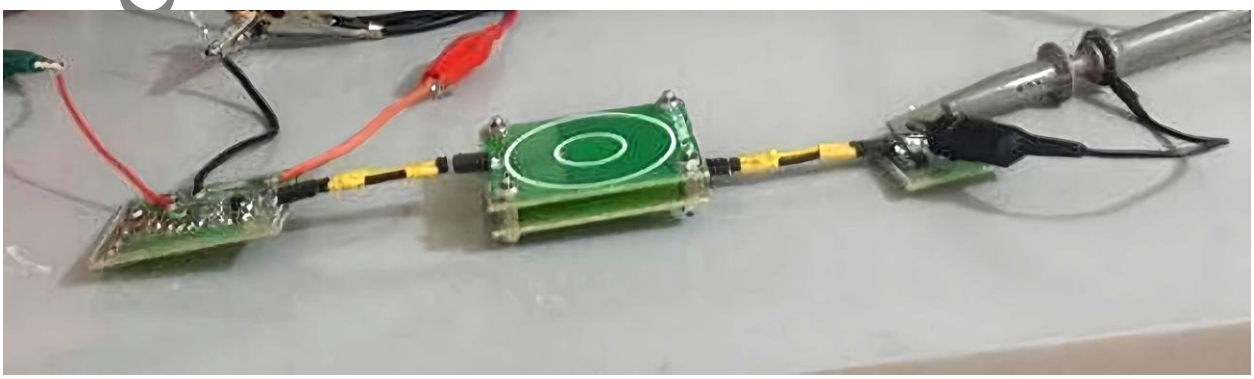

Fig. 6. Optimized coupled coils.

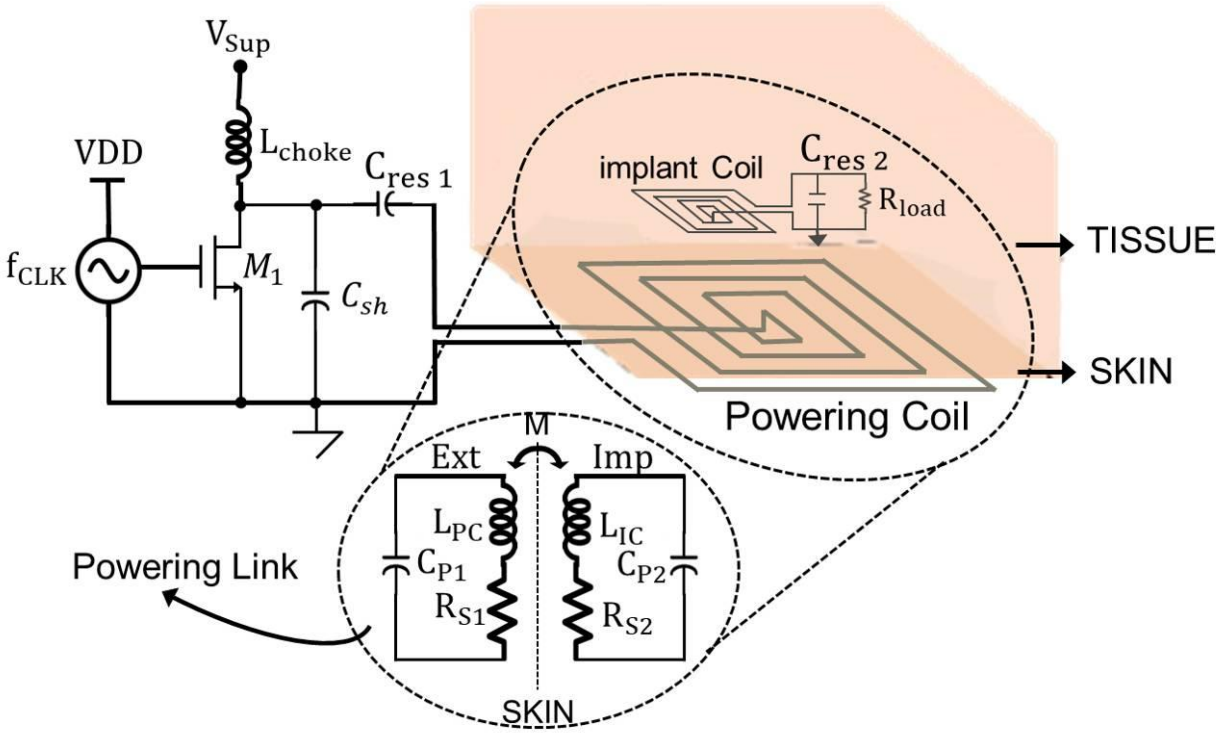

Fig. 7. Magnetically coupled WPT link.

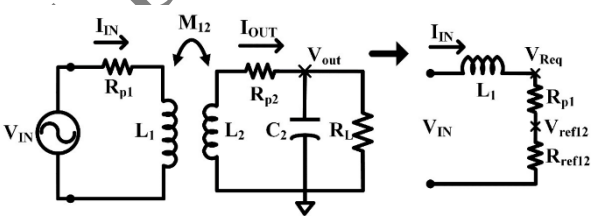

(13)

Fig. 8. Total System Power Transmission

Accepted by

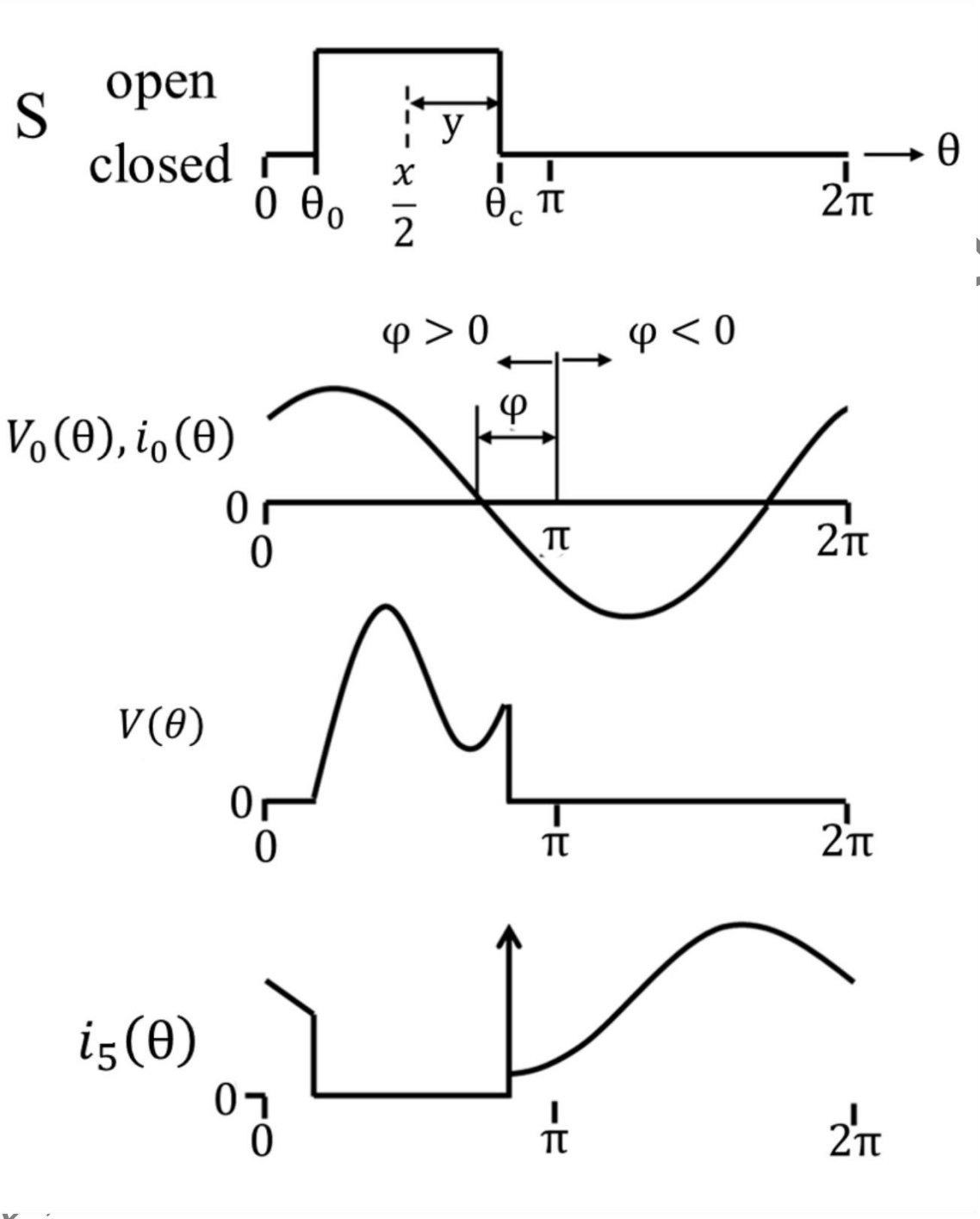

Fig. 9. L_0 and C_0 cannot fully resonate each other.

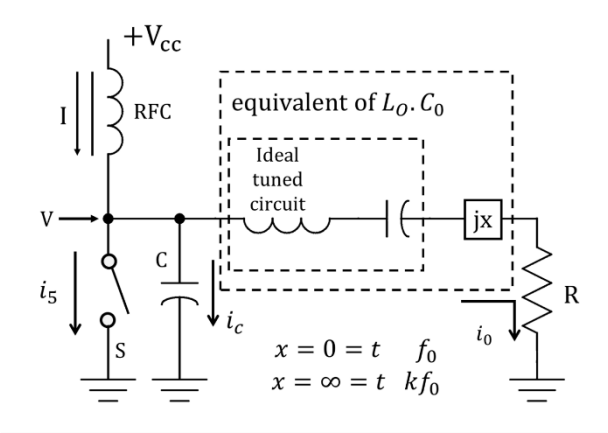

Fig. 10. Completely nonlinear circuit[25].

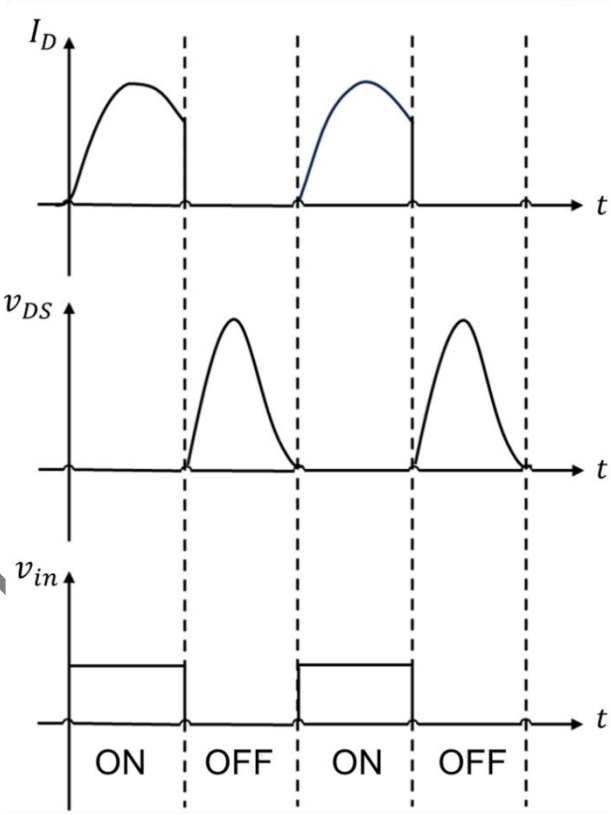

Fig. 11. Voltage-time diagram.

Accepted Iranica

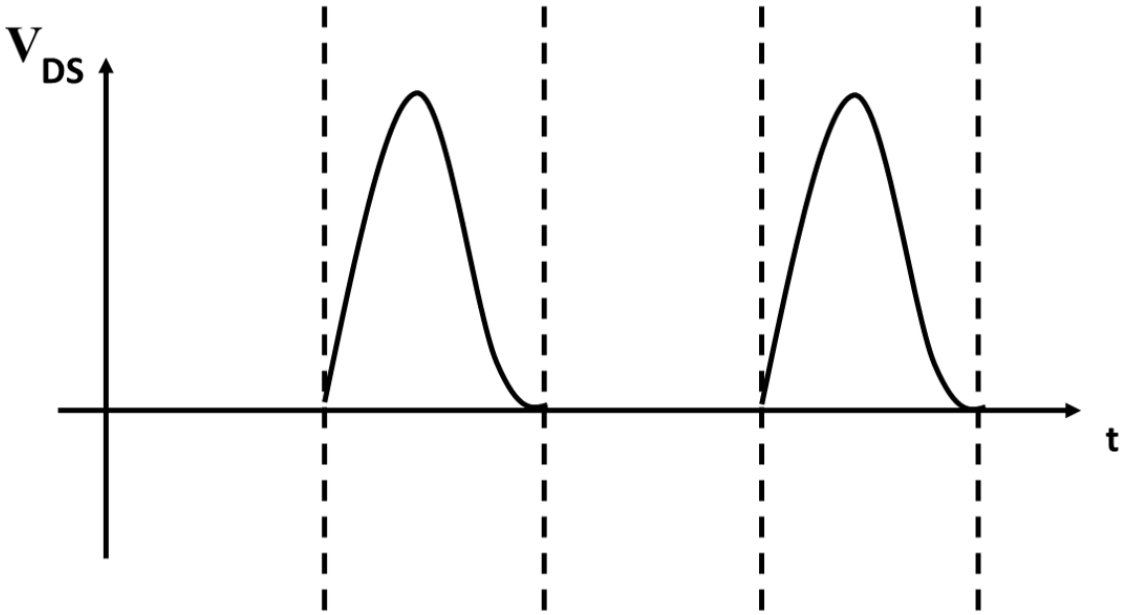

Fig. 12. Voltage slope-time diagram.

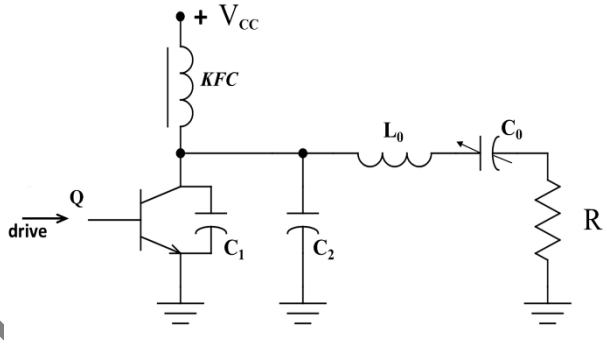

Fig. 13. Transistor resistance R_{ds}.

Accepted manuscript

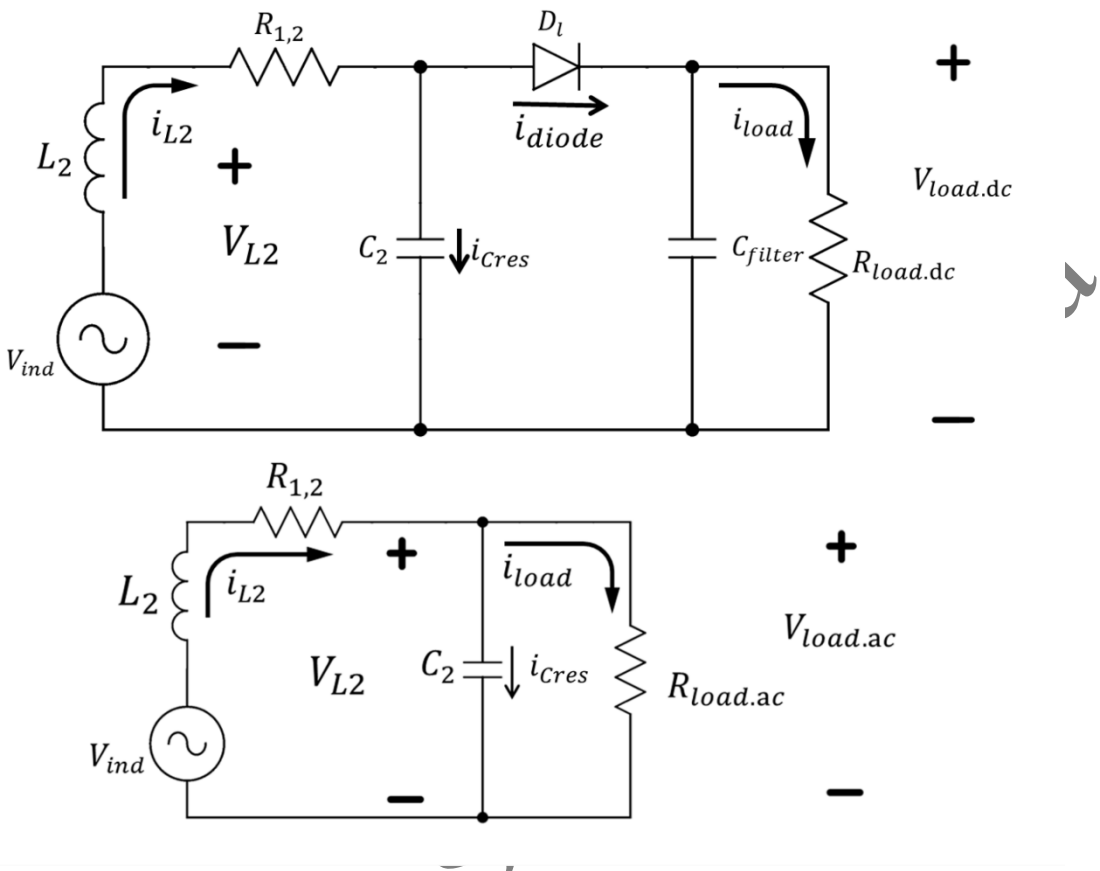

Fig. 14. V_{MAX} on Both Sides of the Collector.

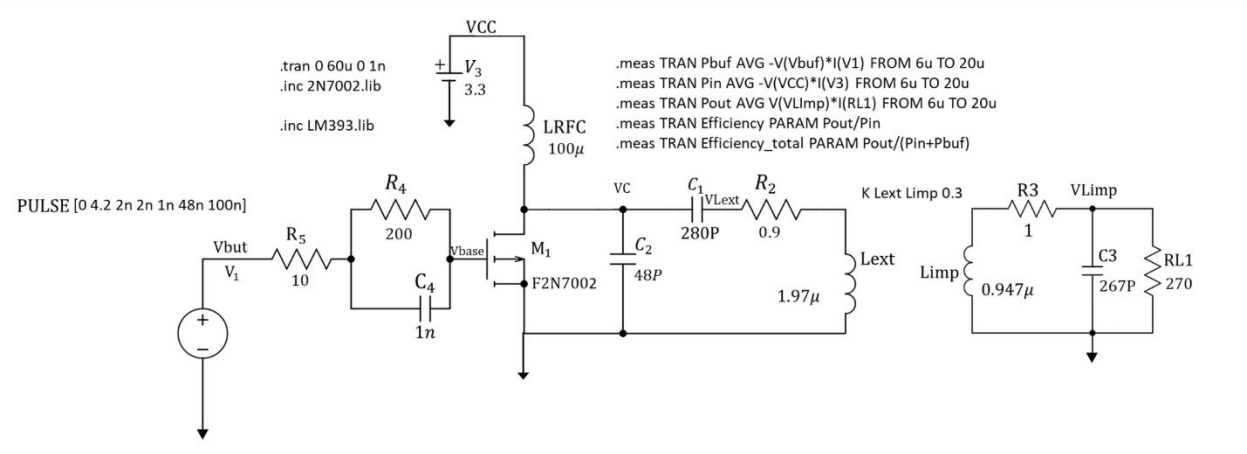

Fig. 15. LTspice simulation circuit.

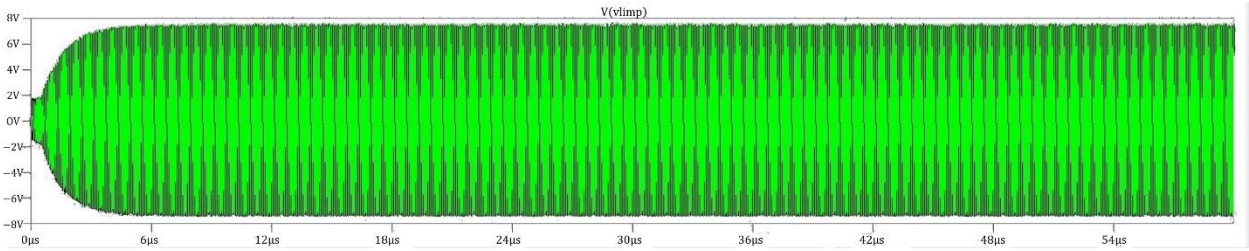

Fig. 16. Simulation output in LTSpice (steady-state region only).

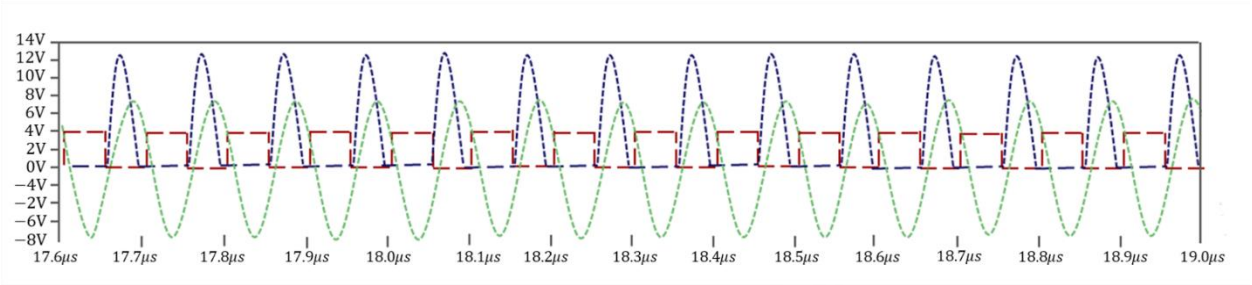

Fig. 17. Transistor voltage (blue) and base voltage (green).

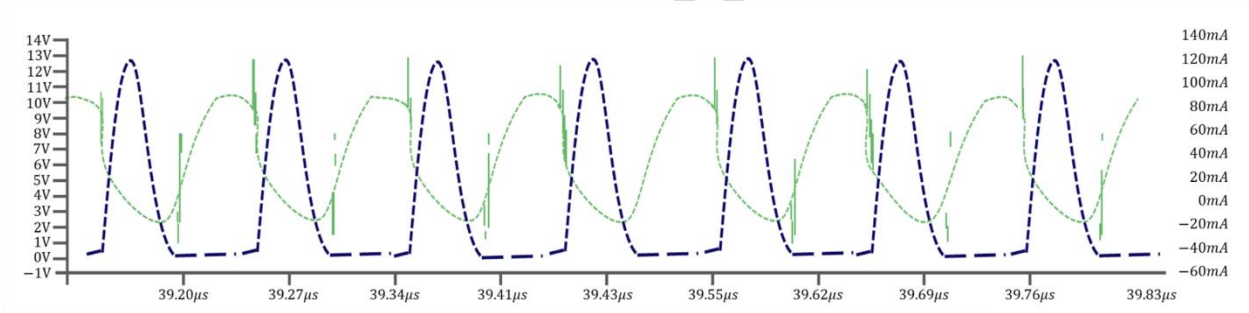

Fig. 18. Transistor current (blue) and base current (green).

Accepted Manuscript

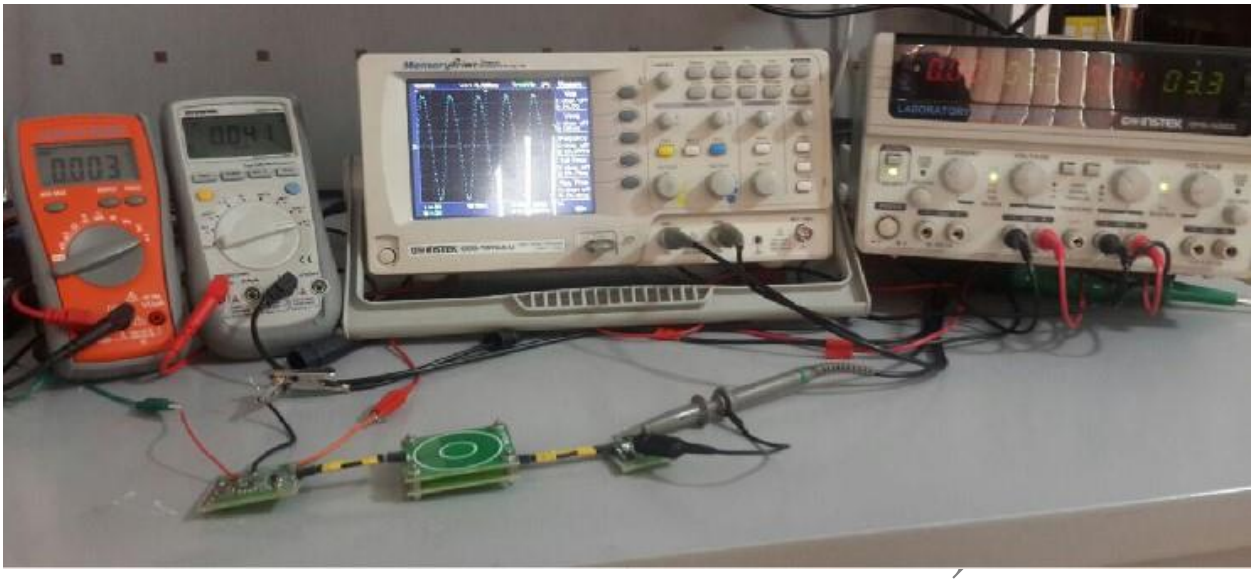

Fig. 19. Experimental test.

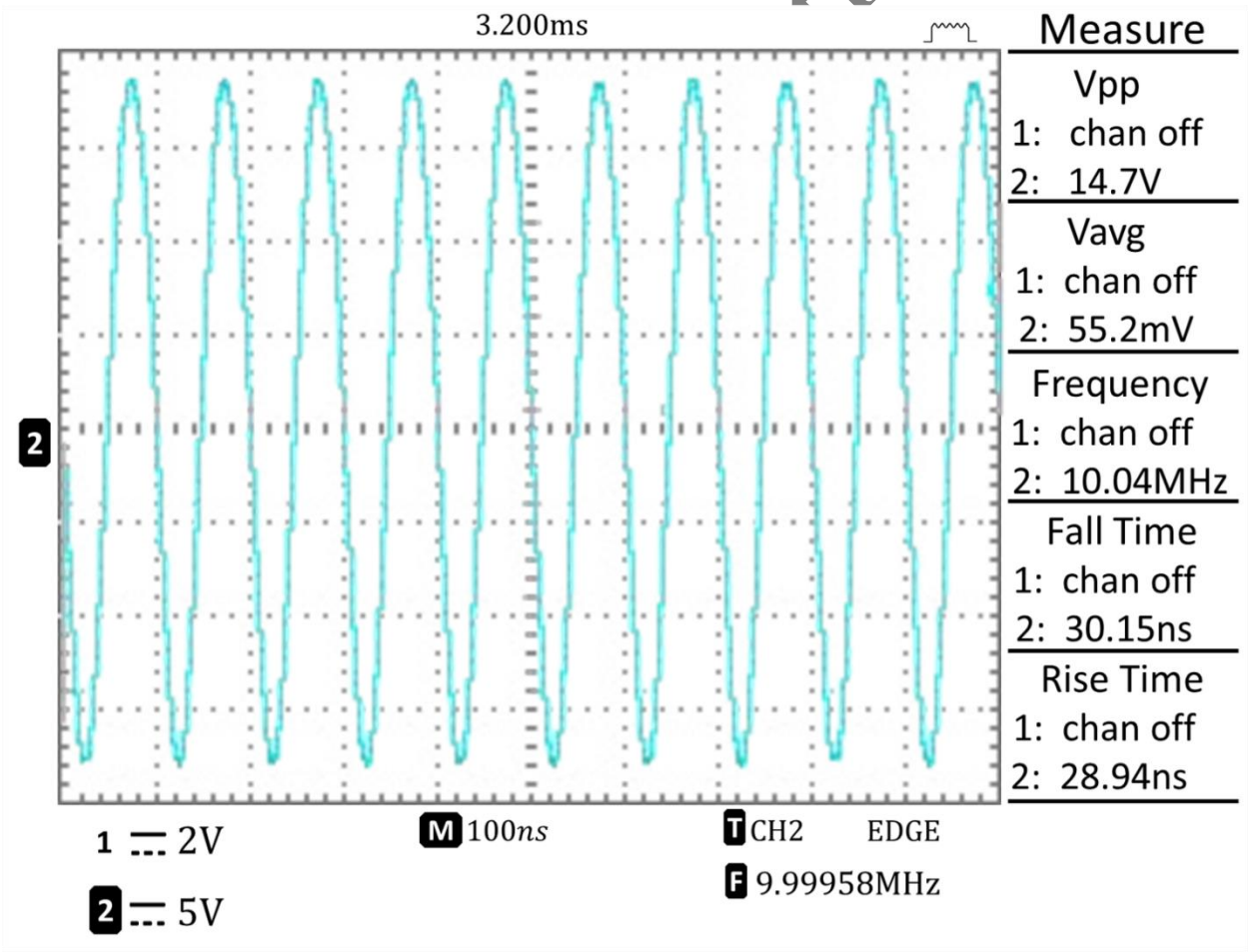

Fig. 20. Sinusoidal output

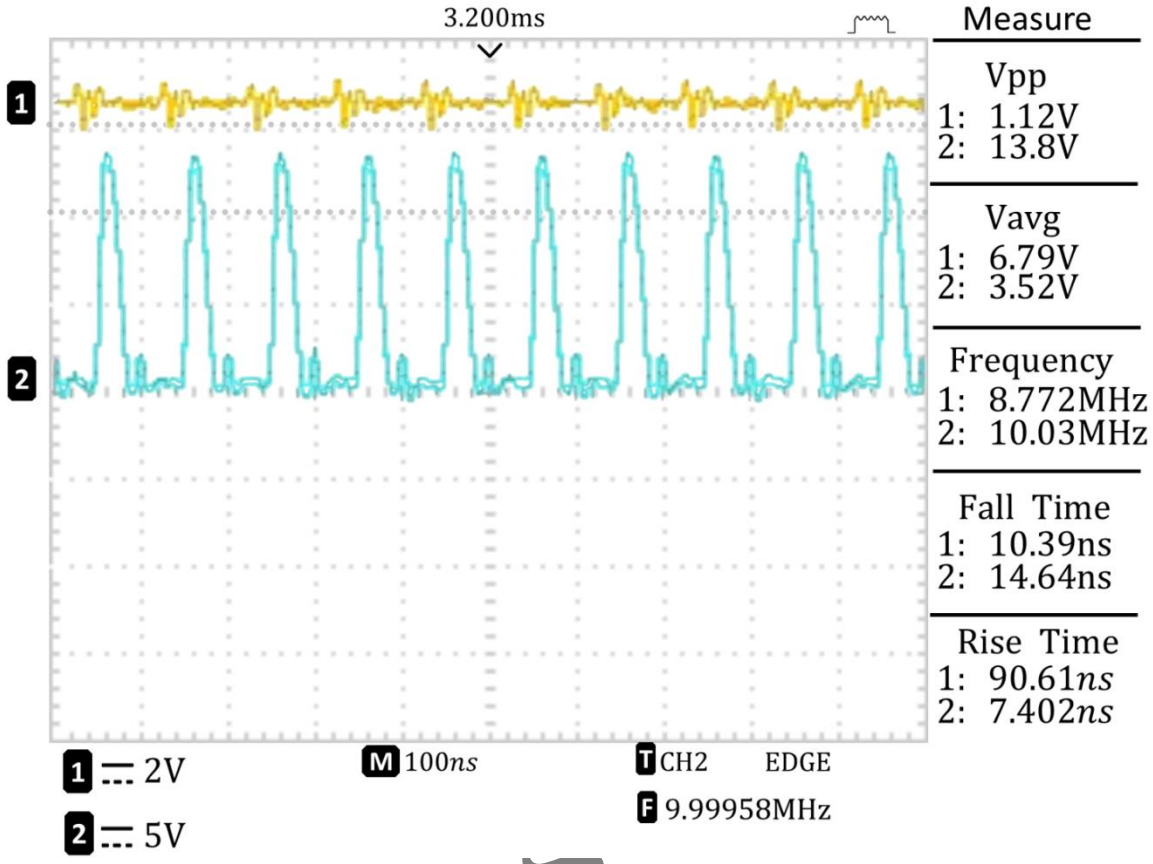

Fig. 21. Base current and voltage.

Table 1. WPT parameters.

Parameter	**Unit**	**Value**
Frequency	MHz	10
Coil spacing	mm	5
Maximum outer diameter	mm	25
Minimum coil spacing	μm	150
Minimum coil width	μm	150
Load resistance	Ω	500

*Copper coil is used on FR4-PCB

Accepted by S

Table ۲. Quantitative comparison of state-of-the-art inductive power transfer solutions for ICD and related implants

Reference	**Year**	**Implant/Device**	**Topology/Coil Type**	**Frequency (MHz)**	**Max Reported**	**Notable Characteristics**

					WPT Efficiency (%)	
Helalian et al.	**2017**	**Cardiac Pacemaker**	**Planar spiral**	**1.5**	**23**	**Dual-coil, bidirectional link**
Lee et al.	**2024**	**Deep Brain Stim.**	**Stacked circular**	**13.56**	**34**	**Miniature secondary coil**
Zhang et al.	**2025**	**ICD**	**Planar mirrored-spiral**	**13.56**	**29**	**High-Q magnetic resonance**
Detka et al.	**2023**	**Cardiac implants**	**Planar coil**	**—**	**23**	**Optimized planar coil**
This work	**2024**	**ICD**	**Optimized coupled spiral**	**10.00**	**51**	**Geometric opt., class-E PA**

Author_Bios_ScientiaIranica

Accepted by Scientia

Bahador Makkiabadi received his B.Sc. degree in Electrical Engineering from Shiraz University, Shiraz, Iran, in 1997. He obtained his M.Sc. and Ph.D. degrees in Biomedical Engineering from Amirkabir University of Technology, Tehran, Iran, and the University of Surrey, Guildford, UK, in 2000 and 2011, respectively. He is currently an Associate Professor at the Department of Medical Physics and Biomedical Engineering, and a member of the Research Center for Biomedical Technology and Robotics (RCBTR), Tehran University of Medical Sciences (TUMS).

His research interests include EEG signal processing and blind source separation of biomedical signals, brain–computer interfaces (BCI), and ultrasound array signal processing and imaging.

Hossein Ahmadi-Danesh-Ashtiani was born in 1971. He received his Ph.D. degree in Energy Engineering in 2004, following his undergraduate studies in Mechanical Engineering. His research interests include energy saving, pinch technology, exergy analysis, fossil fuels, and renewable energies, and he has published several related papers in both English and Persian. He is currently a faculty member at the Department of Mechanical Engineering, Islamic Azad University, South

Ahmad Khoshgard received his B.Sc. degree in Chemical (Petrochemical) Engineering from Amirkabir University of Technology, Tehran, Iran, in 1992, and his M.Sc. degree in Chemical Engineering from Sharif University of Technology, Tehran, Iran, in 1995. He earned his Ph.D. in Energy Systems Engineering from Islamic Azad University in 2004. His research interests include optimization of chemical processes and process integration, energy planning, energy system modeling, and renewable energy systems. He is currently an Assistant Professor at the Department of Chemical Engineering, Islamic Azad University, South Tehran Branch.

Abdollah Hosseinnia is a Ph.D. candidate in Energy Systems Engineering at Islamic Azad University (IAU), South Tehran Branch, Iran. He received his B.Sc. degree in Electrical Engineering and his M.Sc. degree in Energy Systems Engineering in 2015 and 2017, respectively.

Scientia Iranica

His research interests include biomedical array signal processing, wireless power transfer, microsystems, and electronic medical records.

Accepted by Scientia Iranica